Electronic states and modulation doping of hexagonal boron nitride trilayers

Taishi Haga,[1,*] Yuuto Matsuura,[1] Yoshitaka Fujimoto,[1] and Susumu Saito[1,2,3]
[1]*Department of Physics, Tokyo Institute of Technology, 2-12-1 Oh-okayama, Meguro-ku, Tokyo 152-8551, Japan*
[2]*Advanced Research Center for Quantum Physics and Nanoscience, Tokyo Institute of Technology, 2-12-1 Oh-okayama, Meguro-ku, Tokyo 152-8551, Japan*
[3]*Materials Research Center for Element Strategy, Tokyo Institute of Technology, 4259 Nagatsuta-cho, Midori-ku, Yokohama, Kanagawa 226-8503, Japan*

(Received 7 December 2020; revised 7 August 2021; accepted 15 September 2021; published 30 September 2021)

We study the stabilities and geometric and electronic properties of hexagonal boron nitride (*h*-BN) trilayers by using first-principles electronic-structure calculations within the framework of the density functional theory. From the results of total-energy calculations, we reveal the relative stabilities for various stacking sequences of *h*-BN trilayers. We also show that energy-band structures as well as spatial distributions of wave functions at the valence-band maximum (VBM) and the conduction-band minimum (CBM) strongly depend on the stacking sequences of the *h*-BN trilayers. We further investigate the effects of substitutional doping of a carbon atom on the electronic properties of the *h*-BN trilayers. In several stacking sequences of the C-doped *h*-BN trilayers, we find that the C-atom dopant can be spatially separated from the carrier transport layers associated with the VBM or the CBM, suggesting the possibility of realizing conduction channels only weakly disturbed by the C-atom impurity in *h*-BN trilayers. Interestingly, these donor states spatially separated from the CBM state are found to become rather shallow. This theoretical finding of "atomically thin modulation doping" using the *h*-BN layers may open an important way to design future layered electronic device materials.

DOI: 10.1103/PhysRevMaterials.5.094003

I. INTRODUCTION

In 2002, graphene, a monolayer graphite sheet, was theoretically studied to clarify its electronic properties [1] and to construct new carbon-network materials [2] before the experimental synthesis of graphene. Ever since the successful exfoliation of graphene from graphite [3], graphene and other two-dimensional (2D) atomic layered materials have attracted much attention in the nanoscience field due to their unique and novel properties such as the massless Dirac fermion and anomalous quantum Hall effect in graphene [4–7]. Like graphene, hexagonal boron nitride (*h*-BN) has a honeycomb lattice structure composed of alternating boron and nitrogen atoms. It is known that *h*-BN is a wide-gap semiconductor with a large fundamental gap of about 6 eV in its bulk phase [8–11]. On the other hand, few-layer *h*-BN should show much more variation in its electronic properties depending on the number of layers and the stacking sequence. In the case of bilayer graphene, for example, it has two major stacking sequences, *AA* and *AB* stackings, and the electronic structures of the bilayer graphenes with these two stacking sequences are considerably different from each other [12–15]. In the case of *h*-BN, each layer has only a threefold rotational symmetry, unlike the sixfold rotational symmetry of graphene. Hence, few-layer *h*-BN can possess more kinds of stacking sequences than corresponding few-layer graphene and should show rich variations of electronic structures depending on the stacking sequences [16–19]. For example, there are as many as five major stacking sequences in the case of the *h*-BN bilayer, which shows indirect or direct band gap depending on the stacking sequences.

Modulation doping, in which the doped impurities are spatially separated from the carrier transport region, is a key technology in achieving a high carrier mobility of semiconductors [20]. It was theoretically reported that impurity states of *h*-BN layers induced by a substitutional carbon atom appear within a fundamental gap of the *h*-BN layers [21–23]. Experimentally, it was shown that C-atom dopants are incorporated into the *h*-BN layers using secondary ion mass spectrometry measurements [24]. Furthermore, it was reported that substitutional C doping in *h*-BN nanosheets was achieved experimentally via *in situ* electron-beam irradiation inside a transmission electron microscope [25]. In addition, *h*-BN layers with various stacking sequences such as aa' and *ab* stackings are experimentally synthesized and observed [19,26–28]. (Here we follow the expression of the stacking sequence of *h*-BN layers proposed in previous works [29–31] originally for *h*-BN/graphene heterostructures.) Therefore, C-doped and/or undoped layered *h*-BN with various stacking sequences could be selectively produced using the exfoliation of *h*-BN monolayers from *h*-BN bulk material and layer-by-layer stacking techniques [32,33]. The high carrier mobility might be realized by using modulation doping in few-layer *h*-BN.

In this paper, we study the relative stabilities of *h*-BN trilayers with 10 different stable stacking sequences and the effects of C-atom doping on their electronic properties using

*haga.t@stat.phys.titech.ac.jp

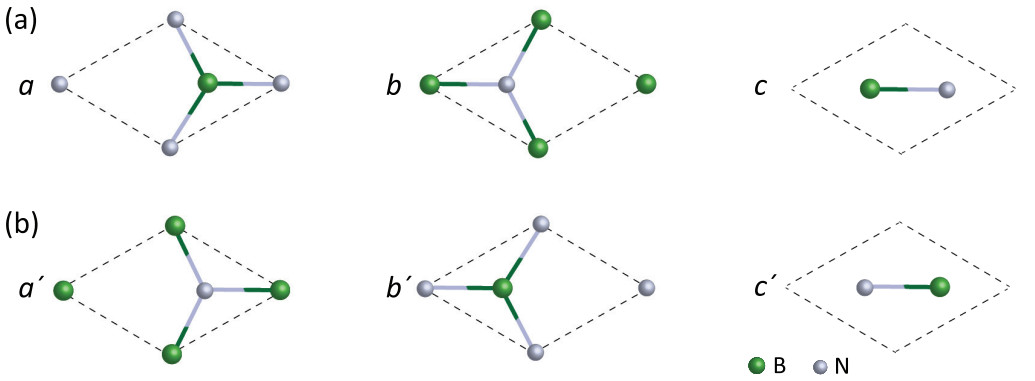

FIG. 1. Nomenclature of stacking sequence for *h*-BN layers: (a) *a*, *b*, and *c* layers and (b) *a*′, *b*′, and *c*′ layers. The dashed line denotes the unit cell of the monolayer sheet. The green and gray balls represent B and N atoms, respectively.

first-principles electronic-structure calculations based on density functional theory (DFT). We show that C-atom doping in the *h*-BN trilayers can give rise to a shallow donor or acceptor state compared with the doping in the *h*-BN monolayer. Furthermore, in the specific stacking sequence of the *h*-BN trilayer, we find that the very shallow donor state appears. We also find that the C-atom dopant is spatially separated from the carrier transport layers in the cases of several stacking sequences of C-doped *h*-BN trilayers, indicating the possibility of modulation doping in a material as thin as trilayer *h*-BN.

II. CLASSIFICATION OF *h*-BN TRILAYERS AND COMPUTATIONAL METHODS

A. Stacking sequences

Figure 1 shows the nomenclature of stacking sequences for *h*-BN layers. The first top layer is now defined as *a*. We obtain layer *b* by shifting layer *a* parallel to the B-N bond direction by one bond length. In our nomenclature, the shift from the B to N direction (to the right in Fig. 1) corresponds to this shifting. Layer *c* is obtained by the same shift from layer *b*. Prime symbols (a′, *b*′, and *c*′) denote interchanging the positions of boron and nitrogen atoms, which corresponds to a 60° rotation of the BN layer around the center of the B_3N_3 hexagon.

Figure 2 shows a schematic view of three examples of the *h*-BN trilayers, the *aa*′*a*, *abc*, and *acb*′ stackings. In the *aa*′*a* stacking, N atoms in the middle layer are between B atoms in the top and bottom layers and vice versa. This *aa*′*a* stacking corresponds to the *h*-BN trilayer exfoliated from the *h*-BN bulk phase [26]. As for the *abc* stacking, the B atom in the middle layer is under the N atom in the top layer but above the center of the hexagon of the bottom layer. Therefore, the top and bottom layers are not equivalent. The *abc* stacking has a structure similar to rhombohedral graphite. As for the *acb*′ stacking, the N atom in the middle layer is under the B atom in the top layer, and the B atom in the bottom layer is under the B atom in the middle layer. In the *acb*′ stacking, a shallow impurity-induced state appears, as will be shown later.

In the pristine system, we study 11 stacking sequences among 21 different high-symmetry stacking sequences of *h*-BN trilayers. It was reported that when the N atoms are aligned along the direction perpendicular to atomic layers (N-N alignment), these structures have longer interlayer distances and higher total energies than other structures in *h*-BN bilayers [18,19,34]. In the case of *h*-BN trilayers, there are 10 stacking sequences which do not have N-N alignment: *aba*, *aca*, *abc*, *abb*′, *acc*′, *aa*′*a*, *acb*′, *aba*′, *aa*′*b*, and *ac*′*a*, and therefore, they are expected to be relatively stable structures. For each structure, we perform structural optimization and discuss their relative stabilities by calculating formation

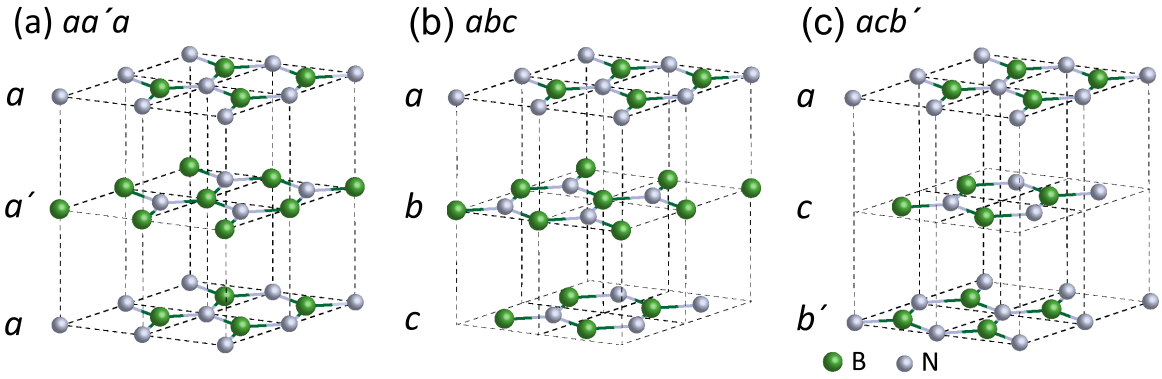

FIG. 2. Schematic view of three different stacking sequences of *h*-BN trilayers: (a) *aa*′*a*, (b) *abc*, and (c) *acb*′. Dashed lines are guides to the eye to indicate relative positions of atoms within the layer and between the adjacent layers.

energies with respect to isolated monolayers as will be given in the next subsection. We show the electronic structure of the *h*-BN trilayers with these stacking sequences in the next section. In addition to these 10 stable structures, in order to estimate the energy difference between stable structures and unstable structures, we study the *aaa*-stacked *h*-BN trilayer, which is expected to be one of the least stable structures due to its N-N-N alignment.

B. Computational methods

The present electronic-structure calculations are performed within the framework of DFT [35,36]. The interactions between ions and the valence electrons are described by ultrasoft pseudopotentials [37]. The cutoff energies for a plane-wave basis set and charge density are taken to be 40 and 400 Ry, respectively. It was reported that the local density approximation (LDA) [38,39] gives reasonable geometries such as in-plane lattice constants and interlayer distances in atomic-layered materials [18,31,40–42]. Nonetheless, we perform calculations using both the LDA and the generalized gradient approximation (GGA) of Perdew, Burke, and Ernzerhof [43] including van der Waals (vdW) interactions by adding the empirical correction scheme called the DFT-D2 [44,45] and compare the LDA and GGA results. The length of the supercell along the direction perpendicular to the 2D layers is taken to be 30 Å for both doped and undoped *h*-BN trilayers. As for the supercell size of the doped trilayers along the direction parallel to the 2D layers, an 8×8 cell size (19.93 Å) is used. For the Brillouin-zone integration, $32 \times 32 \times 1$ and $4 \times 4 \times 1$ *k*-point samplings are used for undoped and doped cases, respectively. In this work, all calculations are performed using the QUANTUM ESPRESSO package [46,47]. We use the VESTA package to describe the distributions of wave functions [48].

The relative stabilities of different stacking sequences are discussed based on the formation energy E_f, which is defined as

$$E_f = E_{\text{tri}} - 3E_{\text{mono}}, \tag{1}$$

where E_{mono} is the total energy of the *h*-BN monolayer and E_{tri} is the total energy of the *h*-BN trilayer, which depends on the stacking sequence.

In this paper, donor and acceptor ionization energies are given as

$$E_D = \varepsilon_{\text{CBM}} - \varepsilon_{\Gamma}^{\text{Donor}}, \tag{2}$$

$$E_A = \varepsilon_{\Gamma}^{\text{Acceptor}} - \varepsilon_{\text{VBM}}, \tag{3}$$

where ε_{CBM}, ε_{VBM}, and $\varepsilon_{\Gamma}^{\text{Donor(Acceptor)}}$ are the Kohn-Sham eigenvalues at the conduction-band minimum, valence-band maximum, and the donor (acceptor) state at the Γ point. These values should be lower than true ionization energies [49]. However, the order of E_D and E_A should be mostly reliable, and moreover, we can identify the shallow impurity-state cases using these values. In this paper, we discuss relative ionization energies using E_D and E_A. For more accurate calculations of the ionization energy, *GW* calculations should be preferable, although the *GW* calculation for the supercell with doped impurities is still too computationally expensive at present.

The energetics of substitutional dopings with C atoms are discussed based on the formation energy of substitutional doping $E_f^{\text{C}_{\text{B(N)}}}$, which is defined as

$$E_f^{\text{C}_{\text{B(N)}}} = E_{\text{tot}} - E_{\text{tri}} - \mu_{\text{C}} + \mu_{\text{B(N)}}, \tag{4}$$

where E_{tot} is the total energy of doped *h*-BN and μ_{C}, μ_{B}, and μ_{N} are chemical potentials of C, B, and N atoms, respectively. These chemical potentials are obtained by using graphene, α-boron crystal, and the N_2 molecule as reference systems.

III. RESULTS AND DISCUSSION

A. Energetics and geometries

Table I shows the optimized interlayer distances and formation energies of *h*-BN trilayers obtained by the LDA and GGA + vdW calculations. The optimized in-plane lattice constants are 2.491 and 2.506 Å in the LDA and GGA + vdW calculations, respectively. Table I shows that the *aba* stacking has the lowest formation energy E_f with the shortest interlayer distance among the 10 kinds of stable stacking sequences studied. We therefore conclude that the *aba* stacking sequence is the most stable one among various stacking sequences of *h*-BN trilayers. On the other hand, the *aaa* stacking has considerably higher formation energy than the other 10 stacking sequences in both LDA and the GGA+vdW calculations. It is found that the formation energy value is lower when interlayer distance is shorter, which is in good agreement with a previous study on bilayer *h*-BN systems [18]. Interestingly, the $aa'a$ stacking is the sixth stable structure among 10 stable stacking patterns, although the $aa'a$ stacking corresponds to the *h*-BN trilayer exfoliated from the *h*-BN bulk phase [26–28]. In the case of bilayer *h*-BN, it was predicted that the *ab*-stacked system is stable based on first-principles calculations [18], and the system was actually synthesized experimentally afterwards [19]. Therefore, the present results for relative stabilities should be reliable as well. In both LDA and GGA + vdW calculations, the relative stabilities of 11 stacking sequences are exactly the same. Importantly, the interlayer distances of the *h*-BN bulk phase in our LDA and GGA + vdW calculations are 3.24 and 3.11 Å, respectively. These values are in good agreement with a previous study [50]. On the other hand, it was reported that the experimental value of the interlayer distance of the *h*-BN bulk is 3.33 Å [51]. The interlayer distance calculated by the LDA methods, 3.24 Å, is much closer to the experimental value than the value calculated by using the GGA + vdW methods, 3.11 Å. When the interlayer distances between *h*-BN layers are much shorter than the experimental value, the interlayer interaction becomes too strong, and consequently, the electronic structure should be incorrect. Therefore, hereafter, we will use the LDA methods for the calculations of the electronic structure. It is now experimentally feasible to make magic angle bilayer graphene with small rotation [52,53]. Therefore, it should be possible to make the "*a* layer" and "a' layer" in *h*-BN with a macroscopic operation.

TABLE I. Interlayer distances and formation energies of *h*-BN trilayers with 11 types of stacking sequences obtained by LDA and GGA + vdW calculations. Two different interlayer-distance values of *abc*, *abb′*, *acc′*, *acb′*, *aba′*, and *aa′b* sequences originate from their geometric asymmetry with respect to the middle layer.

	LDA		GGA + vdW	
Stacking sequence	Interlayer distance (Å)	E_f (meV/cell)	Interlayer distance (Å)	E_f (meV/cell)
aba	3.227	−120.1	3.090	−295.0
aca	3.228	−119.9	3.100	−292.8
abc	3.231/3.227	−119.8	3.102/3.099	−292.7
abb′	3.226/3.246	−118.7	3.099/3.131	−290.3
acc′	3.228/3.255	−118.2	3.101/3.136	−289.1
aa′a	3.247	−117.2	3.130	−287.1
acb′	3.228/3.267	−115.7	3.100/3.159	−283.0
aba′	3.229/3.267	−115.6	3.101/3.161	−282.9
aa′b	3.242/3.280	−114.0	3.136/3.162	−279.5
ac′a	3.268	−111.4	3.159	−273.1
aaa	3.585	−67.95	3.428	−198.8

B. Energy-band structures and wave functions

1. Pristine trilayers

We study the energy-band structures of the 10 stable stacking sequences of the *h*-BN trilayers discussed in the previous section. Figure 3 shows the energy-band structures of the pristine *h*-BN trilayers. All the structures studied are wide-gap semiconductors, although their band structures are quantitatively different. Table II lists band gap values E_g and the transition types of the pristine *h*-BN trilayers. The value of the

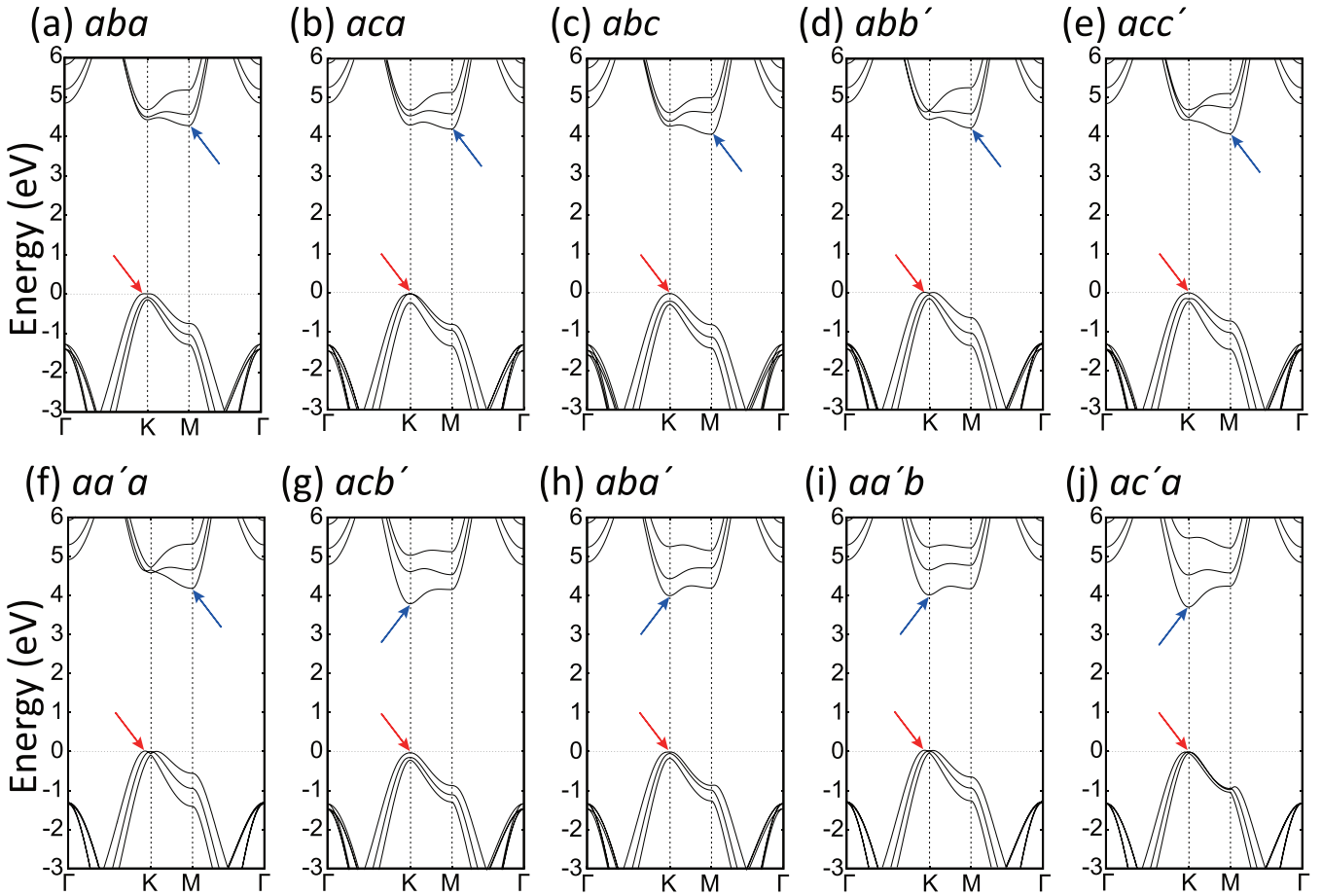

FIG. 3. Energy-band structures of the pristine *h*-BN trilayers. The Fermi level is set to zero. In each case, blue and red arrows indicate the conduction-band minimum and valence-band maximum, respectively. Six sequences [(a) to (f)] possess indirect gaps, while three sequences [(g), (h), and (j)] possess direct gaps. The *aa′b* trilayer in (i) possesses nearly direct gap.

TABLE II. Band gap values and transition types of *h*-BN trilayers with 10 stable stacking sequences.

	Stacking sequence									
	aba	*aca*	*abc*	*abb′*	*acc′*	*aa′a*	*acb′*	*aba′*	*aa′b*	*ac′a*
E_g (eV)	4.27	4.22	4.09	4.20	4.06	4.17	3.82	3.98	3.99	3.73
CBM	M	M	M	M	M	M	K	K	K	K
VBM	Γ-K line	K	K	Γ-K line	K	Γ-K line	K	K	Γ-K line	K
Transition	Indirect	Indirect	Indirect	Indirect	Indirect	Indirect	Direct	Direct	Indirect	Direct

band gap of the *h*-BN monolayer is 4.62 eV, obtained using the LDA calculation. It is found that the band gap values of the *h*-BN trilayers are always smaller than that of the *h*-BN monolayer due to the interlayer interactions among three *h*-BN layers in the system. It is also found that, interestingly, there are sizable differences in the band gap values of the 10 trilayers. For example, the difference between the gap values of the most stable stacking, *aba,* and the third most stable stacking, *abc,* is as large as 0.18 eV. It is interesting that shifting the bottom layer by one boron-nitrogen bond length alone generates this difference, suggesting the possibility of mechanical modifications of the electronic properties in these systems.

The values of band gaps listed in Table II should be lower than experimental values due to the underestimation of the band gaps in LDA. However, the relative values of band gaps and gap types (direct versus indirect gap) are expected to be mostly accurate. We therefore discuss the gap types of these 10 trilayers. It should be noted that the conduction-band minimum (CBM) of the six most stable trilayers with *aba*, *aca*, *abc*, *abb′*, *acc′*, and *aa′a* stackings are located at the M points, while the CBMs of the other stackings are located at the K points. On the other hand, the valence-band maximum (VBM) of the *aca*, *abc*, *acc′*, *acb′*, *aba′*, and *ac′a* stackings are located at the K points, while the VBMs of the other stackings are located near the K points. Hence, the six most stable trilayers possess an indirect gap, while the other four trilayers possess a direct or almost direct gap. Interestingly, changing the stacking of the *h*-BN trilayer from *acc′* to *acb′* leads to an indirect gap to direct gap transition. It is interesting to note that "B-B stacking" may prefer the direct band gap. The VBM is around the K point in any stacking sequence. On the other hand, the CBM is at the K point or the M point. The state at the K point is lowered to become the CBM state in trilayers with a B atom located directly above a B atom, and the systems possess direct gap. This tendency is also seen in the case of bilayer systems [18]. It is therefore revealed that *h*-BN trilayers have various electronic structures depending on their stacking sequences. These variations in the energy-band structures, including band gap energies and their transition types, clearly indicate that band structure engineering via the stacking sequence in *h*-BN layers should actually be possible.

We also study spatial distributions of wave functions of the 10 stable structures. It has been confirmed that neither VBM nor CBM states are degenerate in all 10 stacking sequences studied. Figure 4(a) shows squared wave functions of each structure at the CBM. As shown, the shape of the wave functions reflects π states. The *h*-BN trilayers are geometrically symmetric with respect to the middle layer in the *aba*, *aca*, *aa′a*, and *ac′a* stackings. Therefore, they have a symmetric distribution of squared wave function at the CBM. The other trilayers are geometrically all asymmetric with respect to the middle layer, and so are the squared wave function distributions. Interestingly, in *acb′*, *aba′*, and *aa′b*, the wave function distributions are localized in the bottom two layers at the CBM, and the topmost *a* layer has a low amplitude. In other trilayers, except *abc*, it is also found that the topmost *a* layer has the smallest spatial distribution of the CBM wave function. In the case of the *abc* trilayer, the bottom *c* layer has the lowest amplitude. This nonuniform spatial distribution of the CBM wave function gives rise to an interesting way of doping, which will be discussed later.

Figure 4(b) shows, on the other hand, wave functions of each trilayer at the VBM. At the VBM, as in the case of the CBM, the wave function distributions reflect the geometrical symmetry. The layers with the smallest amplitude are summarized as follows: *b* (*aa′b*), *b′* (*acb′*), *c* (*aca*), *c′* (*ac′c* and *ac′a*), and *a* (the others). Among the 10 stacking sequences studied, 6 trilayers do not have mirror symmetry in the middle layer and are expected to have interlayer polarization. In the case of the *ab*-stacked (*ba*-stacked) bilayer, the interlayer polarization was observed experimentally [54]. Although the definition of the charge of each layer is not straightforward, predicting the polarization is an interesting future issue for these asymmetric trilayers

It should be noted that the wave function can be localized in certain layers when the CBM state is at the K point. The localization of the CBM and VBM states observed might be explained by using the theory proposed previously for the *h*-BN bilayer [55]: the states at the K point should be localized when the BN layer is commensurably shifted without rotation such as the *ab*-stacked bilayer. Even in the trilayer system, the CBM states at the K point are localized in the case of *acb′* and *aba′*, which possess commensurably shifted BN bilayers. On the other hand, the CBM state in the *ac′a* is not localized since it does not have a commensurable shift of BN layers even though the CBM is at the K point. Localized VBM states at the K point observed in *aca*, *abc*, *acc′*, *acb′*, and *aba′* can be explained by the commensurable shift as well.

2. C-doped trilayers

We consider the substitutional doping of the C atom at the B site (C_B) and at the N site (C_N) to induce donor and acceptor states, respectively, and to produce *n*-type and *p*-type trilayers. Since CBM and VBM states can be localized in certain layer(s), doping of C_B and C_N in the layer with the smallest amplitude of the CBM and VBM wave functions, respectively, may spatially separate the carrier conducting layer from the doped layer. Then, the carriers move mostly

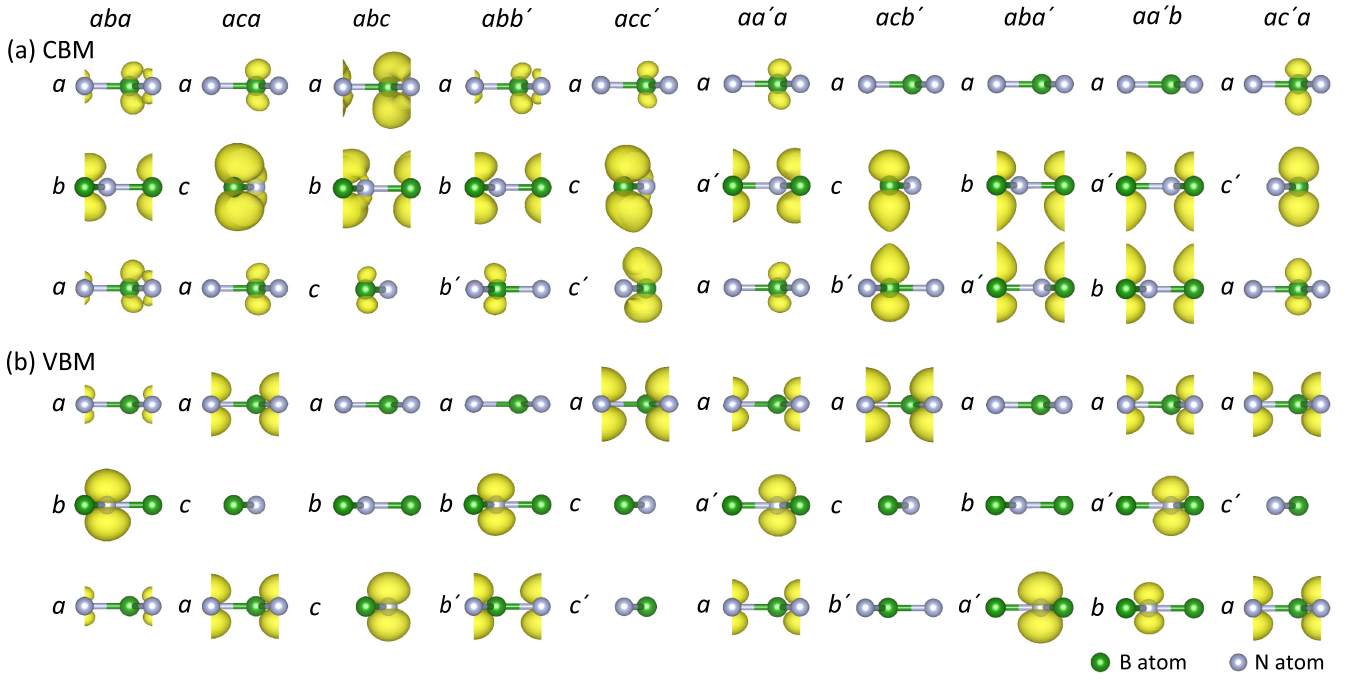

FIG. 4. Isosurfaces of squared wave functions (a) at the CBM and (b) at the VBM for the 10 stable stacking sequences. Isosurface values of the electron density is set to 0.01 electron/bohr^3.

in the perfect layer without impurities, and therefore, in these systems high carrier mobilities should be expected. Hence, we choose C_B and C_N doping layers in all 10 stable trilayers this way. It should be noted that C_B is more energetically favorable than C_N in the case of the *h*-BN monolayer [22,56]. The calculated formation energies for C_B and C_N in the *h*-BN monolayer are found to be 4.31 and 5.04 eV, respectively. These results are in good agreement with our previous work [22]. The calculated formation energies for C_B and C_N in the *abc* stacking are found to be 5.04 and 5.79 eV, respectively. Therefore, the formation energies in the trilayer system are larger than those in the monolayer system, and C_B is more energetically favorable than C_N in the case of *h*-BN trilayer. It is interesting to note that, although the formation energies of C_B and C_N in trilayers are larger than those in monolayer *h*-BN, their difference (0.75 eV) is almost the same as that in the monolayer (0.73 eV).

Figure 5 shows energy-band structures of *h*-BN trilayers with C_B and C_N, respectively. We now express the C_B- and C_N-doped *a* layers by $\overline{a}$ and $\underline{a}$, respectively. In all stacking structures, the donor and acceptor states induced by C_B and C_N appear in the fundamental gap. Table III shows donor and acceptor ionization energies of these doped *h*-BN trilayers. In the case of the *h*-BN monolayer, the ionization energy of C_B was reported to be 0.935 eV in our previous work [22]. The ionization energy of C_N is only slightly less than that of C_B; the difference is less than 0.1 eV in the LDA calculations [22]. Ionization energies of C_B and C_N in a *h*-BN trilayer with any stacking sequence are found to be lower than those of the *h*-BN monolayer. An increasing number of layers leads to a sizable reduction of ionization energies.

Interestingly, $\overline{a}cb'$ has a very shallow donor state. We here consider how the shallow donor state is induced. The wave function of the CBM state of the acb' trilayer does not have any amplitude on the topmost *a* layer, as shown in Fig. 4(a). Figure 6 shows spatial distributions of the wave function of the second-lowest unoccupied state at five points from the K point to the M point in the acb' trilayer. The second-lowest unoccupied state at the K point is mostly localized in the topmost *a* layer, although the state around the M point is also distributed in the bottom b' layer. The impurity state induced by the C atom doped in the *a* layer of the acb' trilayer should be associated with the second-lowest unoccupied state that is mainly distributed in the topmost *a* layer, as shown in Fig. 6. Actually, the donor state should be mostly localized in the topmost *a* layer, as will be shown later. Therefore, the donor state is relatively deep when measured from the second-lowest unoccupied state, while it is shallow when measured from the CBM since the energy difference between the CBM and the second-lowest unoccupied state is rather large (about 0.75 eV, as shown in Fig. 3). Hence, $\overline{a}cb'$ with a shallow donor state is the *n*-type semiconductor. In the case of C_N doping, on the other hand, the splitting of the VBM state is not so large. Nonetheless, it is found that $\underline{a}bc$ has a relatively shallow acceptor state. In the case of acb', the effective mass of an electron m_e at the CBM is $1.02m$; on the other hand, the effective mass of a hole m_h at VBM is $1.52m$ (m is the electron mass). Each effective mass is calculated at $\Gamma \rightarrow$ K. In the case of *abc*, m_e ($\Gamma \rightarrow$ M) and m_h ($\Gamma \rightarrow$ K) are $0.97m$ and $1.50m$, respectively. It was theoretically reported that m_e and m_h of the *h*-BN monolayer are $0.95m$ and $0.82m$, respectively [57]. It is found that the effective mass of the electron at the CBM is lighter than that of the hole at the VBM, in contrast to the case of the *h*-BN monolayer.

We have also performed the spin-polarized density functional calculations using the local spin density approximation

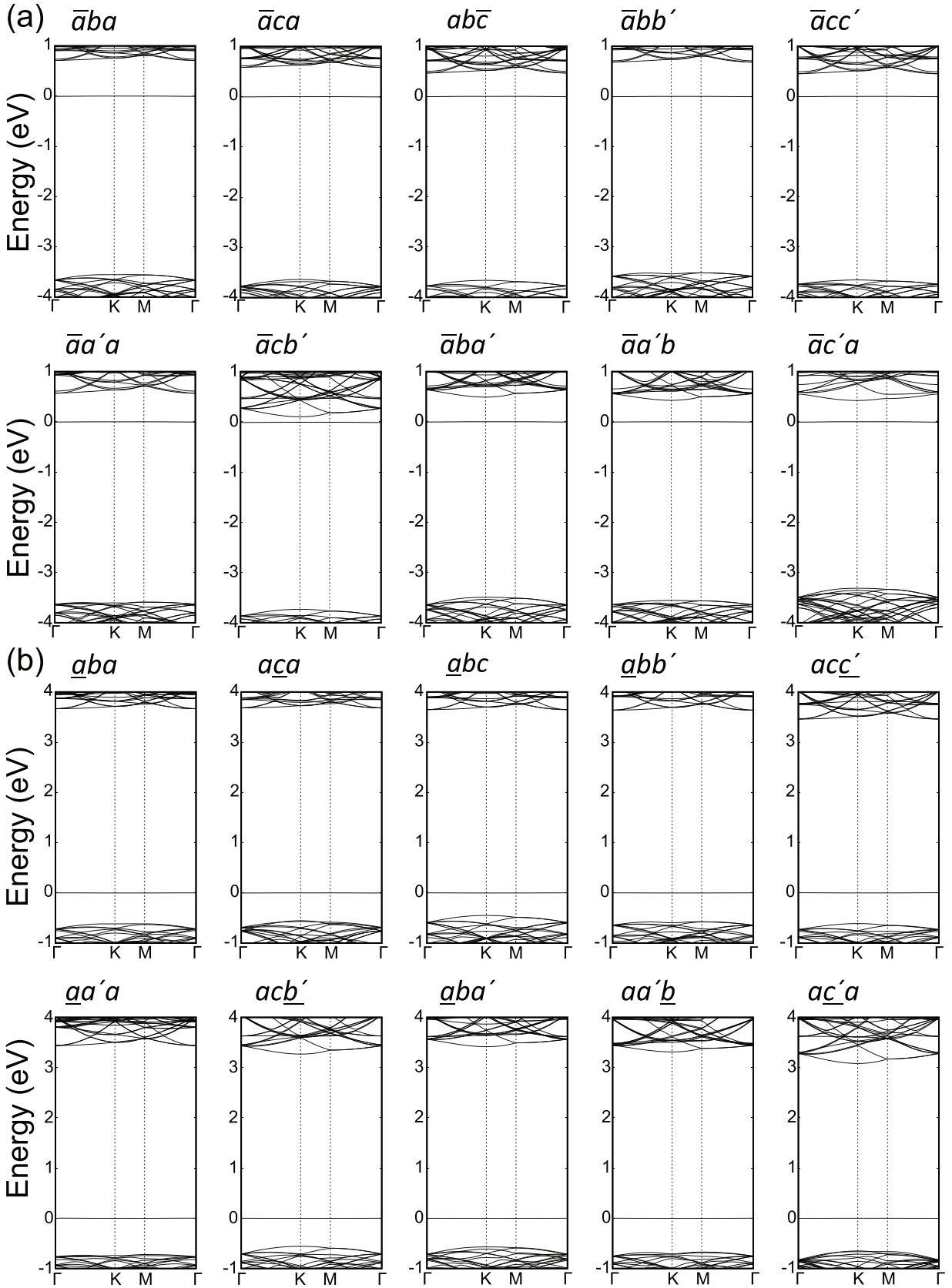

FIG. 5. Energy-band structures of the *h*-BN trilayer with (a) C_B and (b) C_N. The Fermi level is set to zero.

TABLE III. E_D, E_A, and spin-splitting energies $E_{\text{splitting}}$ of h-BN trilayers with C_B and C_N obtained by LDA and LSDA calculations. Overlines and underlines indicate the C-doped h-BN layer at the B site and N site, respectively.

	Stacking sequence (C_B)									
	$\overline{a}ba$	$\overline{a}ca$	$ab\overline{c}$	$\overline{a}bb'$	$\overline{a}cc'$	$\overline{a}a'a$	$\overline{a}cb'$	$\overline{a}ba'$	$\overline{a}a'b$	$\overline{a}c'a$
E_D^{LDA} (eV)	0.71	0.59	0.47	0.69	0.46	0.71	0.11	0.50	0.43	0.43
E_D^{LSDA} (eV)	0.95	0.81	0.73	0.92	0.65	0.79	0.43	0.74	0.60	0.61
$E_{\text{splitting}}$ (eV)	0.54	0.53	0.52	0.54	0.50	0.51	0.55	0.54	0.49	0.43
	Stacking sequence (C_N)									
	$\underline{a}ba$	$a\underline{c}a$	$\underline{a}bc$	$\underline{a}bb'$	acc'	$\underline{a}a'a$	$ac\underline{b}'$	$\underline{a}ba'$	$aa'\underline{b}$	$ac'\underline{a}$
E_A^{LDA} (eV)	0.62	0.55	0.42	0.58	0.61	0.72	0.56	0.57	0.67	0.65
E_A^{LSDA} (eV)	0.89	0.81	0.69	0.92	0.88	0.99	0.84	0.84	0.95	0.93
$E_{\text{splitting}}$ (eV)	0.56	0.53	0.54	0.57	0.56	0.56	0.57	0.55	0.56	0.56

(LSDA) for the C-doped h-BN trilayers. Ionization energies and values of energy splitting, which is defined as the energy difference between impurity-induced spin-up and spin-down states, are listed in Table III. Even considering the spin, the donor state in $\overline{a}cb'$ and acceptor state in $\underline{a}bc$ both have relatively shallow ionization energies. It is found that the values of energy splitting are almost identical for donors and acceptors, except for the C donor in the $\overline{a}c'a$ stacking. Therefore, the energy splitting should be mostly the same in each structure even if the Hubbard U is explicitly considered, like in the LDA+U method, and the relative depth of the impurity-induced state should be the same as given by LDA.

Figure 7 shows the energy-band structures of $\overline{a}cb'$ and $\underline{a}bc$ and undoped acb' obtained using the LSDA calculation. It is evident that doped and undoped band structures are almost the same, except for the impurity-induced state. Therefore, the 8 × 8 supercell is considered to be large enough.

Spin polarization is observed around the impurities in both donor and acceptor cases. In the case of $\overline{a}cb'$, the spin-up state induced by C_B appears 0.43 eV below the CBM. Interestingly, the spin-down state induced by C_B appears in the conduction band. In the case of $\underline{a}bc$, the spin-up and spin-down states induced by C_N appear 0.14 and 0.69 eV above the VBM, respectively. Now, it is not possible to predict the ionization energies of C_B and C_N in each stacking sequence in LDA or LSDA, as discussed in Sec. II B. However, we can discuss the relative magnitudes of ionization energies, which should be mostly reliable in LDA and LSDA. Actually, from both the LDA and LSDA results, $\overline{a}cb'$ is expected to give a shallow donor state.

We now focus on the wave functions of C-doped h-BN trilayer systems. Figure 8(a) shows distributions of wave functions at the CBM states and the donor states in the three selected cases of C-doped h-BN trilayers, $\overline{a}cb'$, $\overline{a}ba'$, and $\overline{a}a'b$. These CBM states of doped systems are mostly identical to those of pristine systems which possess small CBM amplitudes with a topmost a layer, as was discussed previously. Therefore, not only $\overline{a}cb'$ but also $\overline{a}ba'$ and $\overline{a}a'b$ have relatively shallow donor states since both the $\overline{a}ba'$ and $\overline{a}a'b$ trilayers have a relatively large splitting between the CBM and the second-lowest unoccupied state [Figs. 3(h) and 3(i)]. In these three cases, CBM states do not possess spatial distribution of the wave function in the C-doped a layer where the donor states are mostly localized. Therefore, these structures are expected to show high carrier mobility.

In the case of acceptor doping, seven stacking sequences, $a\underline{c}a$, $\underline{a}bc$, $\underline{a}bb'$, acc', $ac\underline{b}'$, $\underline{a}ba'$, and $ac'\underline{a}$, have VBM states which are separated from the C-doped layer as shown in Fig. 8(b). Interestingly, there are several patterns of the carrier conducting layer(s) in these seven stacking sequences. For example, the $a\underline{c}a$ stacking has two carrier conducing layers which are top and bottom a layers, while the carrier conducting layer is only the bottom c layer in the $\underline{a}bc$ stacking trilayer.

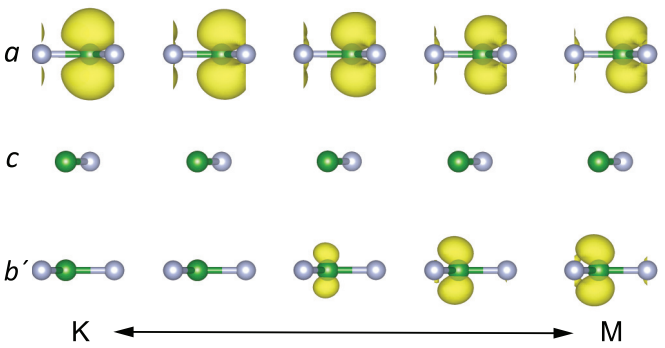

FIG. 6. Isosurfaces of squared wave functions of the second-lowest unoccupied state at five points along the T′ line (from the K point to the M point) in the acb' trilayer. Isosurface values of the electron density is set to 0.01 electron/bohr^3.

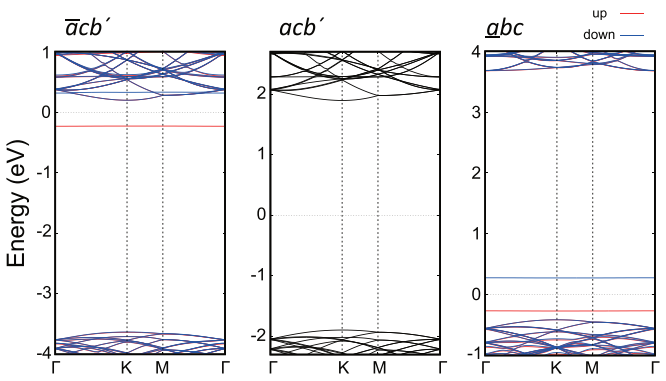

FIG. 7. Energy-band structures of $\overline{a}cb'$, acb' (undoped), and $\underline{a}bc$ obtained by using the 8 × 8 supercell. The Fermi level is set to zero.

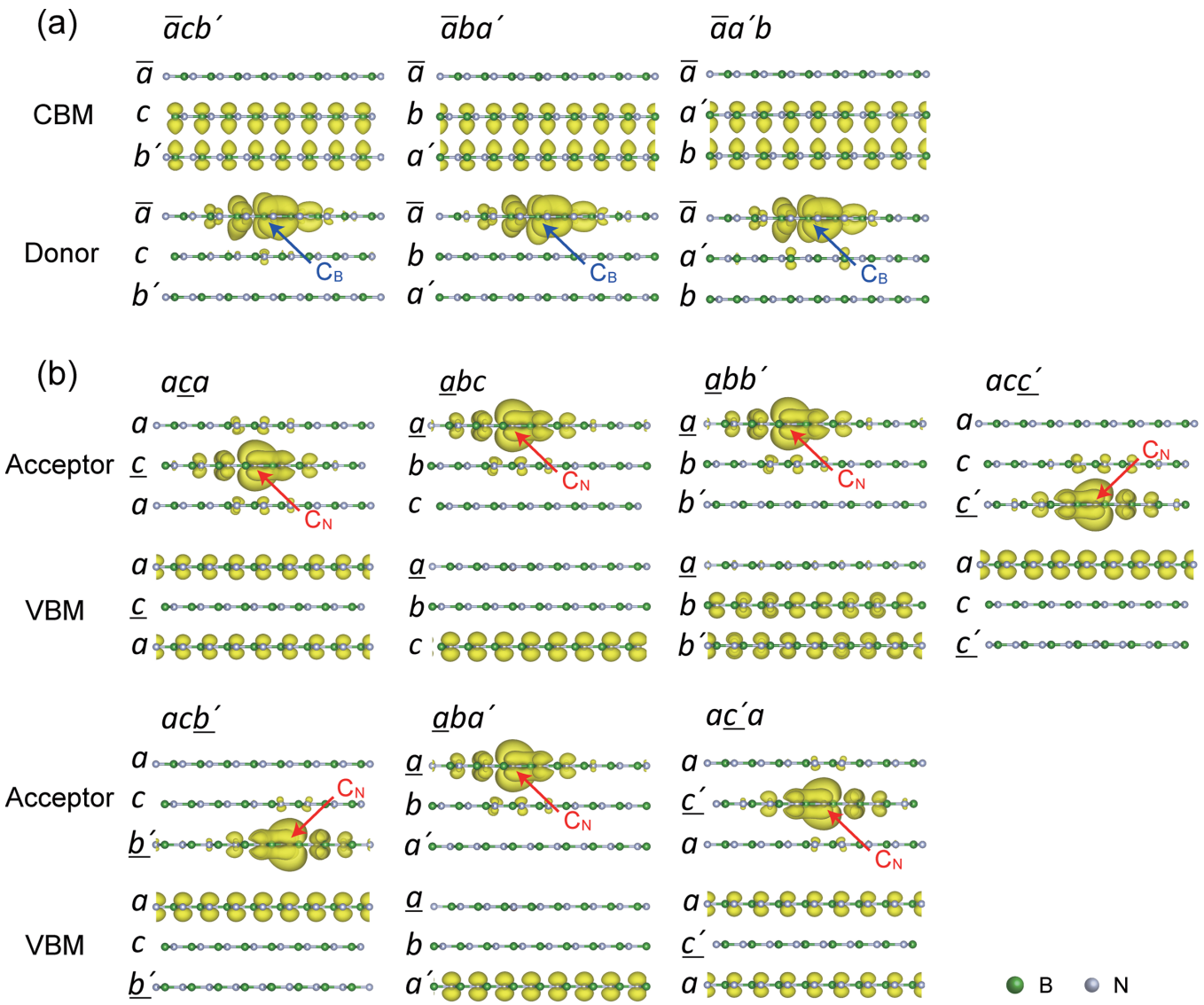

FIG. 8. Isosurfaces of the squared wave functions at (a) the CBM and donor states of three stacking sequences and (b) the acceptor and VBM states of seven stacking sequences. In these trilayers, the conducting layer(s) and the doped layer are spatially separated. The isosurface value of the electron density is set to 0.00016 electron/bohr^3. In each panel, the side view of isosurfaces on one supercell (8×8) is shown with the projected position of C_B (C_N), indicated by the arrow.

Although there are only three types of stacking sequences in the *n*-type trilayers that can possess carrier conducting layers separated from the doped layer, there are as many as seven stacking sequences with such spatial separation in *p*-type trilayers.

In the stable *h*-BN bilayer system which does not include the N-N alignment, modulation doping should be possible in the case of acceptor doping but not in the case of donor doping [58]. By increasing the number of *h*-BN layers, modulation doping becomes possible for both donors and acceptors in the trilayer system. In a system with four or more layers, modulation doping should be possible. This kind of carrier-dopant separation should be considered the ultimate modulation doping with one- or two-atom-thick carrier conducting layers. Furthermore, it should be noted that the modulation doped trilayers should possess shallow impurity-induced donor states, as discussed previously.

IV. SUMMARY

We have clarified the energetics and electronic properties of *h*-BN trilayers by using first-principles calculations based on DFT. The present calculation has confirmed that 10 kinds of stable stacking sequences exist. Interestingly, not the $aa'a$ stacking, but the *aba* stacking, is found to be the most stable in the *h*-BN trilayer system. From the band structures, we have found that these stable *h*-BN trilayers have either an indirect or direct band gap, and the band-gap value depends considerably on its stacking patterns. This rich variation of the electronic structure may open band structure engineering via stacking control in thin *h*-BN layers. We have analyzed the spatial distributions of the wave functions at the CBM and VBM in the 10 stable stacking sequences and found them to have a wide variety of distributions. By substitutional doping of C_B and C_N in the *h*-BN layer with little distribution of

the CBM and VBM states, respectively, we have successfully designed doped *h*-BN trilayers in which the carrier conducting layer(s) and the doped layer are separated from each other. This indicates both electron and hole carriers move in the perfect layer without impurities when the system is thermally excited. Hence, both electron and hole carriers should possess high mobility. Furthermore, we have found that some stacking sequences have relatively shallow impurity-induced states in both donor and acceptor cases. These interesting behaviors are expected to be utilized in future nanoelectronics device materials based on thin *h*-BN layers.

ACKNOWLEDGMENTS

This work was partly supported by the Elements Strategy Initiative to Form Core Research Center, Ministry of Education, Culture, Sports, Science and Technology (MEXT) through the Tokodai Institute for Element Strategy (Grant No. JPMXP0112101001) and Grants-in-Aid for Scientific Research from Japan Society for the Promotion of Science (JSPS) Grants No. JP17K05053, No. JP19H01823, No. JP21K04876, and No. JP25107005. Computations were partly done at the Supercomputer Center of the Institute for Solid State Physics, The University of Tokyo; at the Center for Computational Materials Science, Institute for Materials Research, Tohoku University for the use of MASAMUNE-IMR; and at the Global Scientific Information and Computing Center of the Tokyo Institute of Technology. T.H. also acknowledges the financial support from the Tokyo Tech Academy for Convergence of Materials and Informatics.

[1] Y. Zheng and T. Ando, Phys. Rev. B **65**, 245420 (2002).
[2] T. Matsumoto and S. Saito, J. Phys. Soc. Jpn. **71**, 2765 (2002).
[3] K. S. Novoselov, A. K. Geim, S. V. Morozov, D. Jiang, Y. Zhang, S. V. Dubonos, I. V. Grigorieva, and A. A. Firsov, Science **306**, 666 (2004).
[4] K. S. Novoselov, A. K. Geim, S. V. Morozov, D. Jiang, M. I. Katsnelson, I. V. Grigorieva, S. V. Dubonos, and A. A. Firsov, Nature (London) **438**, 197 (2005).
[5] L. Lindsay and D. A. Broido, Phys. Rev. B **84**, 155421 (2011).
[6] I. Jo, M. T. Pettes, J. Kim, K. Watanabe, T. Taniguchi, Z. Yao, and L. Shi, Nano Lett. **13**, 550 (2013).
[7] A. K. Geim and I. V. Grigorieva, Nature (London) **499**, 419 (2013).
[8] X. Blase, A. Rubio, S. G. Louie, and M. L. Cohen, Phys. Rev. B **51**, 6868 (1995).
[9] K. Watanabe, T. Taniguchi, and H. Kanda, Nat. Mater. **3**, 404 (2004).
[10] B. Arnaud, S. Lebègue, P. Rabiller, and M. Alouani, Phys. Rev. Lett. **96**, 026402 (2006).
[11] G. Cassabois, P. Valvin, and B. Gil, Nat. Photonics **10**, 262 (2016).
[12] C. L. Lu, C. P. Chang, Y. C. Huang, J. H. Ho, C. C. Hwang, and M. F. Lin, J. Phys. Soc. Jpn. **76**, 024701 (2007).
[13] M. Aoki and H. Amawashi, Solid State Commun. **142**, 123 (2007).
[14] A. A. Avetisyan, B. Partoens, and F. M. Peeters, Phys. Rev. B **81**, 115432 (2010).
[15] W. Bao, L. Jing, J. Velasco, Y. Lee, G. Liu, D. Tran, B. Standley, M. Aykol, S. B. Cronin, D. Smirnov, M. Koshino, E. McCann, M. Bockrath, and C. N. Lau, Nat. Phys. **7**, 948 (2011).
[16] R. M. Ribeiro and N. M. R. Peres, Phys. Rev. B **83**, 235312 (2011).
[17] G. Constantinescu, A. Kuc, and T. Heine, Phys. Rev. Lett. **111**, 036104 (2013).
[18] Y. Fujimoto and S. Saito, Phys. Rev. B **94**, 245427 (2016).
[19] S. M. Gilbert, T. Pham, M. Dogan, S. Oh, B. Shevitski, G. Schumm, S. Liu, P. Ercius, S. Aloni, M. L. Cohen, and A. Zettl, 2D Mater. **6**, 021006 (2019).
[20] M. Weidner, A. Fuchs, T. J. M. Bayer, K. Rachut, P. Schnell, G. K. Deyu, and A. Klein, Adv. Funct. Mater. **29**, 1807906 (2019).
[21] N. Berseneva, A. Gulans, A. V. Krasheninnikov, and R. M. Nieminen, Phys. Rev. B **87**, 035404 (2013).
[22] Y. Fujimoto and S. Saito, Phys. Rev. B **93**, 045402 (2016).
[23] T. J. Smart, F. Wu, M. Govoni, and Y. Ping, Phys. Rev. Mater. **2**, 124002 (2018).
[24] T. Taniguchi and K. Watanabe, J. Cryst. Growth **303**, 525 (2007).
[25] X. Wei, M.-S. Wang, Y. Bando, and D. Golberg, ACS Nano **5**, 2916 (2011).
[26] R. S. Pease, Nature (London) **165**, 722 (1950).
[27] N. Alem, R. Erni, C. Kisielowski, M. D. Rossell, W. Gannett, and A. Zettl, Phys. Rev. B **80**, 155425 (2009).
[28] J. H. Warner, M. H. Rummeli, A. Bachmatiuk, and B. Buchner, ACS Nano **4**, 1299 (2010).
[29] Y. Sakai, T. Koretsune, and S. Saito, Phys. Rev. B **83**, 205434 (2011).
[30] T. Haga, Y. Fujimoto, and S. Saito, Jpn. J. Appl. Phys. **58**, SIIB03 (2019).
[31] T. Haga, Y. Fujimoto, and S. Saito, Phys. Rev. B **100**, 125403 (2019).
[32] S. Masubuchi, M. Morimoto, S. Morikawa, M. Onodera, Y. Asakawa, K. Watanabe, T. Taniguchi, and T. Machida, Nat. Commun. **9**, 1413 (2018).
[33] S. Masubuchi, E. Watanabe, Y. Seo, S. Okazaki, T. Sasagawa, K. Watanabe, T. Taniguchi, and T. Machida, npj 2D Mater. Appl. **4**, 3 (2020).
[34] N. Marom, J. Bernstein, J. Garel, A. Tkatchenko, E. Joselevich, L. Kronik, and O. Hod, Phys. Rev. Lett. **105**, 046801 (2010).
[35] P. Hohenberg and W. Kohn, Phys. Rev. **136**, B864 (1964).
[36] W. Kohn and L. J. Sham, Phys. Rev. **140**, A1133 (1965).
[37] D. Vanderbilt, Phys. Rev. B **41**, 7892 (1990).
[38] D. M. Ceperley and B. J. Alder, Phys. Rev. Lett. **45**, 566 (1980).
[39] J. P. Perdew and A. Zunger, Phys. Rev. B **23**, 5048 (1981).
[40] Z. Zhang, X. C. Zeng, and W. Guo, J. Am. Chem. Soc. **133**, 14831 (2011).
[41] Y. Sakai, S. Saito, and M. L. Cohen, Phys. Rev. B **89**, 115424 (2014).
[42] S. Hemmatiyan, M. Polini, A. Abanov, A. H. MacDonald, and J. Sinova, Phys. Rev. B **90**, 035433 (2014).
[43] J. P. Perdew, K. Burke, and M. Ernzerhof, Phys. Rev. Lett. **77**, 3865 (1996).
[44] S. Grimme, J. Comput. Chem. **27**, 1787 (2006).

[45] V. Barone, M. Casarin, D. Forrer, M. Pavone, M. Sambi, and A. Vittadini, J. Comput. Chem. **30**, 934 (2009).
[46] P. Giannozzi *et al.*, J. Phys.: Condens. Matter **21**, 395502 (2009).
[47] P. Giannozzi *et al.*, J. Phys.: Condens. Matter **29**, 465901 (2017).
[48] K. Momma and F. Izumi, J. Appl. Crystallogr. **44**, 1272 (2011).
[49] T. Koretsune and S. Saito, Phys. Rev. B **77**, 165417 (2008).
[50] G. Graziano, J. Klimeš, F. Fernandez-Alonso, and A. Michaelides, J. Phys.: Condens. Mattter. **24**, 424216 (2012).
[51] V. Solozhenko, G. Will, and F. Elf, Solid State Commun. **96**, 1 (1995).
[52] Y. Cao, V. Fatemi, S. Fang, K. Watanabe, T. Taniguchi, E. Kaxiras, and P. Jarillo-Herrero, Nature (London) **556**, 43 (2018).
[53] Y. Cao, V. Fatemi, A. Demir, S. Fang, S. L. Tomarken, J. Y. Luo, J. D. Sanchez-Yamagishi, K. Watanabe, T. Taniguchi, E. Kaxiras, R. C. Ashoori, and P. Jarillo-Herrero, Nature (London) **556**, 80 (2018).
[54] K. Yasuda, X. Wang, K. Watanabe, T. Taniguchi, and P. Jarillo-Herrero, Science **372**, 1458 (2021).
[55] R. Akashi, Y. Iida, K. Yamamoto, and K. Yoshizawa, Phys. Rev. B **95**, 245401 (2017).
[56] N. Berseneva, A. V. Krasheninnikov, and R. M. Nieminen, Phys. Rev. Lett. **107**, 035501 (2011).
[57] F. Ferreira, A. J. Chaves, N. M. R. Peres, and R. M. Ribeiro, J. Opt. Soc. Am. B **36**, 674 (2019).
[58] T. Haga, Y. Fujimoto, and S. Saito (unpublished).